Pergamon

PII: S0301-9322(96)00067-5

Int. J. Multiphase Flow Vol. 23, No. 2, pp. 301–311, 1997

0301-9322/97 $17.00 + 0.00

HEAT TRANSFER TO TWO-PHASE SLUG FLOWS UNDER REDUCED-GRAVITY CONDITIONS

L. B. FORE[1], L. C. WITTE[2] and J. B. MCQUILLEN[3]

[1]Department of Chemical Engineering, University of Houston, Houston, TX 77204, U.S.A.
[2]Department of Mechanical Engineering, University of Houston, Houston, TX 77204, U.S.A.
[3]NASA Lewis Research Center, Cleveland, OH, U.S.A.

(Received 12 January 1996; in revised form 8 September 1996)

Abstract—New hydrodynamic and heat transfer measurements are presented for two-phase slug flows in a reduced gravity environment. Air and two liquids, water and 50% aqueous glycerine were used to obtain a range of liquid Reynolds numbers from 1000 to 20,000 in a 25.4 mm i.d. tube. The measurements include void fraction, pressure gradient, and heat transfer coefficient. The enhancement of the heat transfer coefficient over single-phase liquid flow increases with increasing void fraction and is somewhat larger for the 50% glycerine solution than for water. Based on a comparison to normal-gravity correlations, the heat transfer coefficients are smaller at reduced-gravity than at normal-gravity under the same flow conditions. This can be explained by smaller liquid-phase turbulence levels in the absence of buoyancy-induced slip between the gas and liquid. © 1997 Elsevier Science Ltd. All rights reserved.

Key Words: two-phase flow, slug flow, two-phase heat transfer, microgravity

1. INTRODUCTION

Two-phase flow occurs in a variety of situations relevant to space operations, such as thermal management and power generation. Gas–liquid slug flow is distinguished by an alternating pattern of bullet-shaped Taylor bubbles and liquid slugs, with large fluctuations in local void fraction, pressure drop and heat transfer. Under normal gravity, buoyancy plays a major role in the hydrodynamics and phase distribution of slug flow. Under reduced gravity, these characteristics are significantly different, so it is reasonable that heat transfer characteristics should also deviate from earth-normal behavior.

Several experimental studies have been performed on reduced-gravity two-phase flows. In addition to developing flow pattern maps and transition criteria (Dukler *et al.* 1988; Zhao and Rezkallah 1993; Bousman and Dukler 1994), detailed measurements of void fraction and pressure drop in slug flow have been performed (Bousman 1994). Rite and Rezkallah (1994) performed one of the only two-component heat transfer studies, a sensible heating experiment for air–water in a 9.53 mm i.d. tube. Their measured heat transfer coefficients were larger or smaller than those obtained under normal gravity by 10–15%, depending on flow conditions.

This paper presents new hydrodynamic and heat transfer measurements for slug flow in a reduced gravity environment. Measurements of void fraction, pressure drop, and heat transfer coefficient were made over a range of gas and liquid flow rates and compared to existing ground-based correlations to illustrate any gravity-dependent differences. New correlations are also developed to better represent the physical behavior.

2. EXPERIMENTAL

Reduced gravity, with a magnitude less than 1% of earth normal, is created aboard NASA's Zero-G KC-135 aircraft by a series of parabolic trajectories. The aircraft climbs and descends between altitudes of 7.6 and 10.6 km over the Gulf of Mexico, achieving reduced gravity for approximately 23 s at the crest of each trajectory. The experiments reported here were performed in October 1994, using test sections designed at the University of Houston and a flow loop designed and fabricated at Lewis Research Center.

2.1. Flow loop

The flow loop, which is shown in figure 1, was aligned parallel to the longitudinal axis of the aircraft. The liquid and gas were supplied to the test section by an air-driven piston within a feed tank and compressed air bottles, respectively. The liquid flow rate was measured with a turbine flow meter and the gas flow rate was measured with an orifice meter. The liquid entered the test section along the inner periphery of the tube through an annular slot in the gas–liquid mixer. The gas entered axially through the center of the mixer. At the downstream end of the test section, the liquid and gas exited into a separator, where the gas was vented off and the liquid collected for recycle in the periods between trajectories.

The adiabatic sections between the mixer and the heated section and between the heated section and the outlet were constructed of 25.4 mm i.d. clear acrylic tubing. The heated section was constructed of 25.9 mm i.d. copper tubing, with nylon end-flanges machined to make a smooth transition to the acrylic tubing i.d. Two pressure taps for the pressure gradient measurement were located upstream of the heated section at locations 1.33 and 1.96 m from the inlet, for an average of 65 tube diameters. A void fraction probe was located at the second pressure tap. The heated test section was located 2.11 m from the inlet and had an overall length of 0.73 m, including the adiabatic end-flanges. The exit section leading to the separator was 0.51 m long.

2.2. Test section and measuring techniques

The axial pressure gradient was estimated between the two pressure stations with two pressure transducers. Pressure reference lines from each transducer were connected in common to the outlet of the test section to keep the measured pressures within the 6900 Pa range. Before each run, liquid was purged through the pressure taps into the test section to remove any trapped air bubbles. The void fraction was estimated with a parallel-wire conductance probe. This probe consisted of a pair of 0.076 mm diameter 13% Rh-Pt wires, stretched across the tube diameter and separated by 3 mm. The conditioning circuitry, described in detail by Lacy and Dukler (1994), output a voltage proportional to the amount of liquid between the two wires.

The heated section is depicted in detail in figure 2. The copper tube, with a wall thickness of 1.27 mm, was plated with nickel and grounded to reduce interference with the conductance probes. The outside of the tube was wrapped with three 36 Ohm (nominal) etched-foil nickel resistance heaters, connected in parallel to 120 V, 60 Hz AC power aboard the aircraft. The heaters covered all but a 1 cm strip along the length of the copper tube. The axial wall temperature profile was measured in that strip with eight 50 Ohm nickel RTDs cemented to the outside of the tube. Vinyl tape was used to secure the heaters and cover the RTDs, and an acrylic box enclosed the heater-tube assembly, serving both as a mount for electrical connections and as insulation against ambient heat loss. An Analog Devices 2B31J strain-gage circuit was used to measure the RTD resistances. The

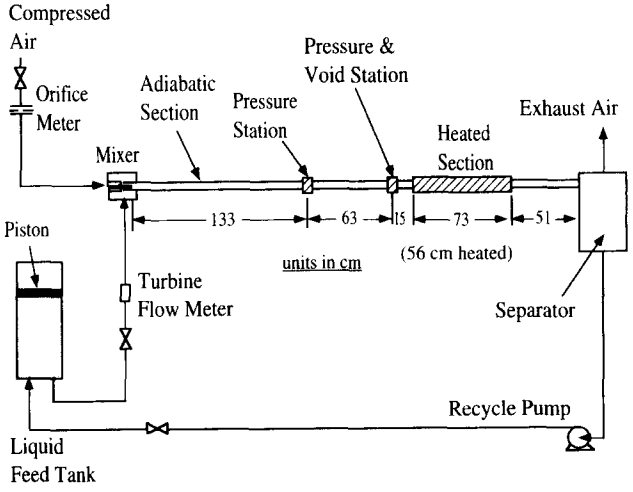

Figure 1. KC-135 flow loop.

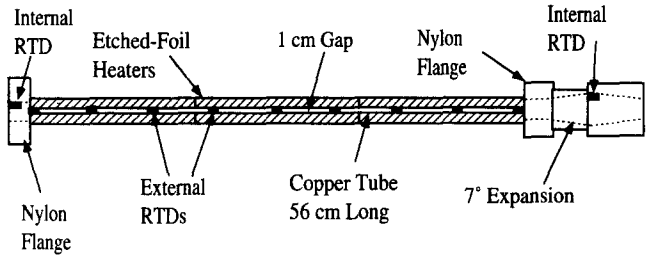

Figure 2. Schematic of heated test section.

entrance bulk temperature was estimated with a nickel RTD mounted inside the nylon flange at the heater entrance. Another RTD, mounted in a special expansion section downstream of the heater, was used as a check on the exit bulk temperature as determined with an enthalpy balance.

The two pressures, void fraction, eight wall temperatures and inlet and outlet temperatures were collected at 1 kHz. Accelerations along three axes at two positions along the flow loop were also collected at 1 kHz. Miscellaneous test section temperatures, gage pressures, and flow rates were collected at 1 Hz.

2.3. *Temporal response*

For most of the successful experiments, gas and liquid flows were started prior to the reduced-gravity period. For the lower velocity conditions, this was required for the two-phase mixture to reach the measuring stations before or shortly after the start of the 20 s recording period. In addition to transients in flow rates and pressure level immediately following flow initiation, the changing gravity level affects the time required to reach a hydrodynamic steady state by altering the distribution of the two phases. This, in turn, increases the time required to reach a thermal steady state in the heated section. The thermal steady state is also affected by the heaters, which require a very short time to warm up, and the copper tube, which has a much larger thermal mass. With no water present, the average tube temperature can increase at a maximum rate of 4.4°C/s at the experimental power level.

Data corresponding to poor gravity levels were eliminated from analysis using the recorded accelerations. Under acceptable gravity levels, less than about 0.01 g, the average pressures reached steady values 2–5 s after the flow rates reached steady values. The wall temperatures along the heated tube, however, required a much longer time to become steady, a problem that has been addressed previously by Rite and Rezkallah (1993, 1994) for similar experiments. Figure 3 presents a typical set of wall temperature time series for one experiment, air–water at a liquid superficial velocity of $U_{LS} = 0.54$ m/s and gas superficial velocity of $U_{GS} = 0.4$ m/s. From this figure, it is obvious that the wall temperature farthest downstream did not quite reach its asymptotic value

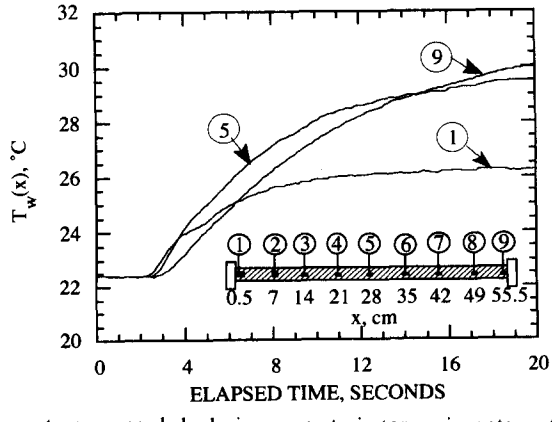

Figure 3. Wall temperatures recorded during one trajectory air–water at $U_{LS} = 0.54$ m/s and $U_{GS} = 0.4$ m/s.

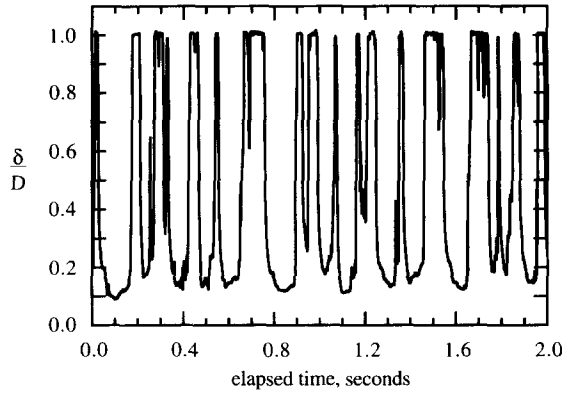

Figure 4. Time series of conditioned void fraction probe output.

within the experimental period. The crossover of temperature time series occurs because wall temperatures farther downstream take longer to reach steady values.

2.4. Data reduction

The output of the conductance monitoring circuit is related directly to the amount of conducting liquid between the void fraction wires, the equivalent height of which is represented by δ. A typical time series of δ/D, the instantaneous line-average fraction of the diameter filled with liquid, is shown in figure 4. For a uniform distribution of bubbles across the tube diameter, the instantaneous void fraction is equal to

$$\epsilon^* = \left(1 - \frac{\delta}{D}\right). \quad [1]$$

When the liquid occupies a contiguous region adjacent to the wall, such as along a Taylor bubble, the instantaneous void fraction is equal to

$$\epsilon^* = \left(1 - \frac{\delta}{D}\right)^2. \quad [2]$$

Full liquid pipe flow is used as a reference to account for temperature-dependent conductivity changes among runs. For slug flows, [1] applies for the liquid slugs when bubbles are present, and [2] applies for the Taylor bubbles. For the present conditions, the Taylor bubbles represent most of the void fraction, so the more accurate equation [2] was used to calculate the instantaneous void fraction, which was averaged over time to obtain the mean void fraction, ϵ.

Using time series such as those shown in figure 3, the steady wall temperatures were estimated for each run by averaging over the last few seconds of the experimental period, at which the wall temperatures were near asymptotic values. Depending on flow conditions, both the averaging period and wall temperatures varied widely among experiments. The local bulk temperature, T_B, was estimated from an enthalpy balance on the liquid as

$$T_B = T_{IN} + \frac{q_w x}{\Gamma C_p}, \quad [3]$$

where T_{IN} is the measured inlet temperature, q_w is the mean wall heat flux, Γ is the mass flow per unit perimeter, and C_p is the specific heat. The local temperatures and axial position, x, were placed in dimensionless forms for convenience in analyzing the local Nusselt numbers, $Nu = hD/k$, from which the local heat transfer coefficients, $h = q_w/(T_w - T_B)$, were back-calculated.

Several examples of local Nusselt numbers calculated in this manner are shown in figure 5. The larger Nusselt numbers correspond to wall-to-bulk temperature differences that are smaller and more difficult to measure accurately. However, the scatter is relatively small along the heated length and the asymptotic Nusselt numbers fairly easy to interpret from an average taken near the tube

exit. In the case of obvious deviations from the norm, such as when wall temperatures were far from steady values, local measurements were discarded from the average. This typically included one or both of the two locations farthest downstream.

2.5. *Error analysis*

There are several potential sources of error in these experiments, such as a lack of flow development and a nonuniform wall heat flux. The flow loop was arranged to maximize the length of the adiabatic section at 83 tube diameters so that the flow would be developed prior to heating. The time-averaged wall heat flux for this experimental system was determined to be uniform with falling-film experiments on the ground (Fore and Witte 1995). Nylon's low thermal conductivity makes the end-flanges effective insulators, so any axial conduction from the ends of the heated tube into them can be neglected. A temperature gradient along the length of the tube implies an axial heat flow within the tube wall. Axial conduction within the wall, flowing from the hotter outlet to cooler inlet, was estimated to be less than 0.2% of the input power along the thermally-developed length, so it is also neglected as a source of uncertainty.

Uncertainties in the measured and calculated quantities were estimated with the propagation of uncertainty method (Moffat 1988), assuming sampling periods long enough to obtain stationary means. The relative uncertainty in the asymptotic heat transfer coefficient is dominated by the uncertainty in the wall heat flux, $\pm 7\%$, which is the same as the uncertainty in the input power. The 1 cm unheated strip had no effect on falling-film experiments, so it is neglected here as a source of uncertainty. The relative uncertainty in the liquid Reynolds number ($\mathrm{Re_L} = 4\Gamma/\mu$) is $\pm 5\%$ for water and $\pm 6\%$ for 50% glycerine, based on errors in the estimated viscosity and measured flow rate. Similarly, the relative uncertainty in the liquid Prandtl number ($\mathrm{Pr} = C_p\mu/k$) is $\pm 2\%$ for water and $\pm 4\%$ for 50% glycerine, based on errors in the viscosity and thermal conductivity. The relative uncertainty in the gas Reynolds number, $\mathrm{Re_G}$, was estimated as $\pm 9\%$, based on errors in flow rate and density.

The uncertainty in the axial pressure gradient, $-\Delta P/L$, was estimated as ± 150 Pa/m, based on the rated $\pm 1\%$ accuracy of the pressure transducers and distance between pressure taps. For the range of measured pressure gradients, this represents relative uncertainties between ± 9 and 23%. Other conditions, such as the presence of bubbles in the pressure taps and insufficient sampling time, increase this uncertainty. The wetted portion of the void fraction wires is accurate to within ± 0.05 mm, based on the accuracy of the calibration and compensation for conductivity changes. This translates to an uncertainty in average void fraction of ± 0.004, a maximum of $\pm 2\%$ over the range of void fractions reported here.

3. RESULTS

Sodium chloride was added to the liquids to increase their electrical conductivities, with nominal weight concentrations of 0.1% for water and 0.6% for 50% glycerine. The average wall heat flux

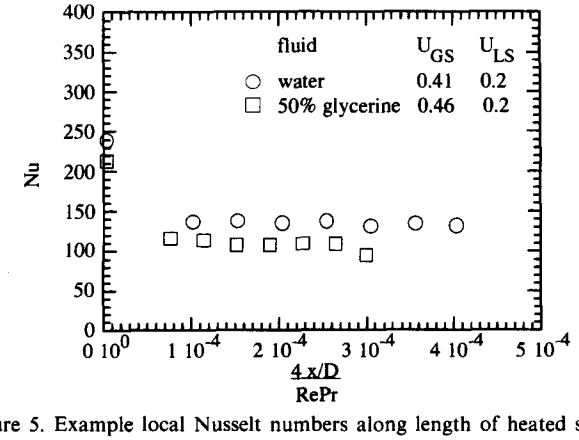

Figure 5. Example local Nusselt numbers along length of heated section.

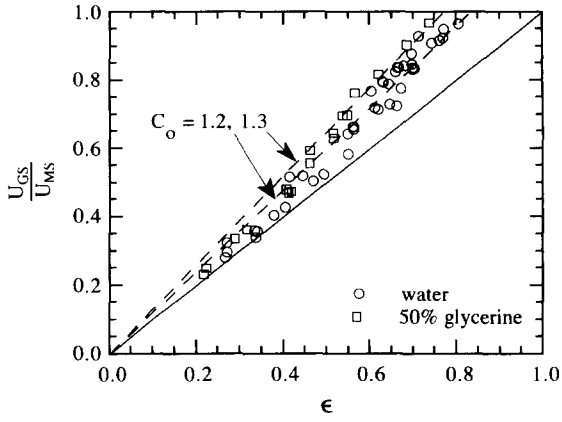

Figure 6. Void fraction measurements correlated with drift–flux model.

was 18,700 W/m^2, which was determined on the ground with approximately the same supply voltage.

The averages for pressure and void fraction were taken only over portions of the time series where the flow rates were steady and the mean acceleration was less than about 0.1 m/s^2. The liquid Reynolds number, which ranged between 1000 and 20,000, was calculated with physical properties evaluated at the exit bulk liquid temperature. The liquid Prandtl number, with nominal ($T = 20°C$) values of 6 for water and 36 for 50% glycerine, was also calculated with physical properties evaluated at the exit bulk liquid temperature. The wall Prandtl number, Pr_w, was calculated with physical properties evaluated at the exit wall temperature. The gas Reynolds number, which ranged between 40 and 4000, was calculated with physical properties evaluated at the mean test section temperature and pressure.

3.1. *Void fraction*

The void fraction measurements are plotted in figure 6 according to the drift–flux model (Zuber and Findlay 1965),

$$\frac{U_{GS}}{U_{MS}} = C_0 \epsilon, \qquad [4]$$

where $U_{MS} = U_{GS} + U_{LS}$. Without buoyancy, the mean drift velocity used in vertical normal-gravity flows is neglected. In figure 6, U_{GS}/U_{MS} is only slightly greater than ϵ at the lowest void fractions of around 0.2, signifying a nearly homogeneous condition. As ϵ increases, C_0 increases to values between 1.2 and 1.3, which is very similar to the behavior of vertical slug flows under earth-normal gravity and consistent with other reduced-gravity results (Dukler *et al.* 1988; Bousman 1994). This measurement of void fraction is a cross-sectional average, so any differences in local values between reduced- and normal-gravity flows cannot be determined from the current set of data.

3.2. *Heat transfer coefficients*

Several correlation methods have been used for two-phase heat transfer coefficients under earth-normal gravity. One method correlates the enhancement over single-phase liquid heat transfer,

$$\eta = \frac{h}{h_L}, \qquad [5]$$

with either the void fraction (Kudirka *et al.* 1965; Dorresteijn 1970), the gas-to-liquid velocity ratio (Shah 1981), or the Lockhart–Martinelli parameter,

$$\phi_L^2 = \frac{\Delta P}{\Delta P_L} \qquad [6]$$

(Fried 1954; Vijay *et al.* 1982). The single-phase liquid heat transfer coefficient, h_L, and pressure

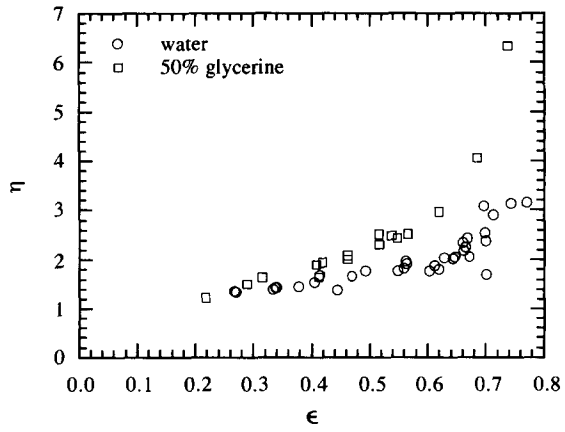

Figure 7. Two-phase heat transfer enhancement vs void fraction.

drop, ΔP_L, are determined from standard heat transfer and friction factor correlations assuming a single-phase liquid flow at the same Reynolds number. The two-phase heat transfer enhancement obtained in the present study is plotted versus ϵ in figure 7. The single-phase heat transfer coefficient was estimated with the Sieder and Tate (1936) turbulent correlation using the experimental Reynolds and Prandtl numbers. In general, the enhancement over single-phase heat transfer approaches unity at zero void fraction, increases with increasing void fraction, and is larger for 50% glycerine than for water. For similar liquid velocities, Rite and Rezkallah (1994) found similar values of η in their reduced gravity experiments. At higher liquid velocities, they found a decrease in the magnitude of η at the same air mass quality.

Vijay *et al.* (1982) developed η-correlations based on ϕ_L^2 for a large number of ground-based vertical experiments. Figure 8 compares the current set of data to the Vijay *et al.* correlation for upward slug flows. Measurements for which the uncertainty in the pressure gradient exceeded $\pm 15\%$ are not included. Most of the data lie below the correlation, with the exception of a few of the 50% glycerine runs. The level of scatter on this plot is quite large, but the water data definitely fall below the correlation line. Elamvaluthi and Srinivas (1984) used the sum of liquid and gas Reynolds numbers to correlate experimental Nusselt numbers. The form of their correlation is

$$\mathrm{Nu} = A(\mathrm{Re_L} + \mathrm{Re_G})^n \mathrm{Pr}^{1/3} \left(\frac{\mu_G}{\mu_L}\right)^{1/4} \left(\frac{\mathrm{Pr}}{\mathrm{Pr_w}}\right)^{0.14}, \qquad [7]$$

with constants of $A = 0.5$ and $n = 0.7$ obtained for mixed Reynolds numbers over the same range

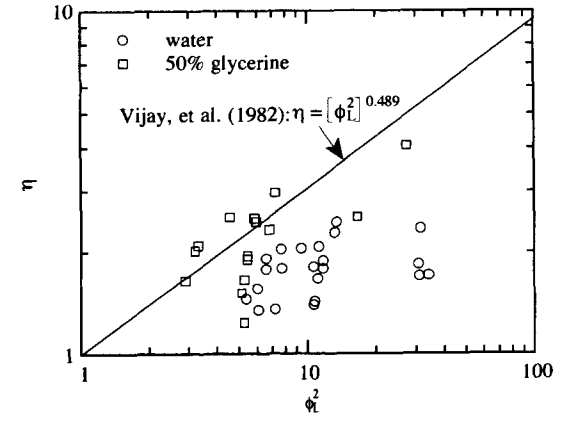

Figure 8. Comparison of two-phase heat transfer enhancement with Vijay *et al.* (1982) correlation for slug flow.

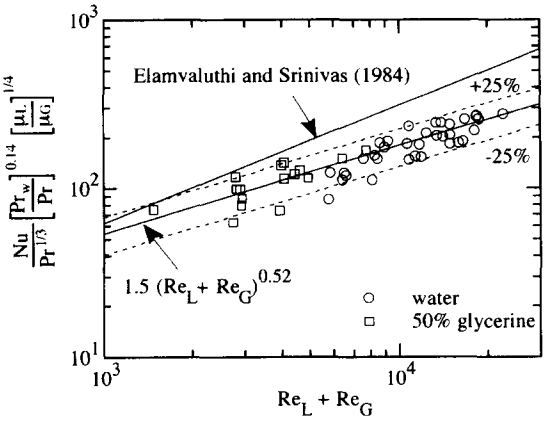

Figure 9. Correlation of slug flow Nusselt numbers with Elamvaluthi & Srinivas (1984) formulation.

as the current set of experiments. The current data are plotted in this form in figure 9, with the best fit occurring for $A = 1.5$ and $n = 0.52$. All of the reduced-gravity data lie below the normal-gravity correlation, suggesting lower Nusselt numbers under the same gas and liquid flow conditions.

Chu and Jones (1980) used a two-phase Reynolds number based on the mean void fraction,

$$\mathrm{Re_{TP}} = \frac{\mathrm{Re}}{(1-\epsilon)}, \qquad [8]$$

to correlate Nusselt numbers in a form similar to the Sieder–Tate correlation. The form of their correlation is

$$\mathrm{Nu} = A\ \mathrm{Re_{TP}^{n}}\ \mathrm{Pr}^{1/3}\left(\frac{\mathrm{Pr}}{\mathrm{Pr_w}}\right)^{0.14}\left(\frac{\mathrm{P_a}}{\mathrm{P}}\right)^{0.17}, \qquad [9]$$

where P_a is atmospheric pressure and P is the local pressure. For the Chu and Jones experiments, $n = 0.55$ for both vertical upflows and downflows with mixed Reynolds numbers between 40,000 and 600,000. The constant, A, varies slightly between upflow and downflow as 0.43 and 0.47, respectively. The current data are plotted in the form of [9] in figure 10 with the Chu and Jones curves included for comparison. The best fit occurs for $A = 0.14$ and $n = 0.62$. Like the comparisons with the Vijay *et al.* and Elamvaluthi and Srinivas correlations, this comparison implies lower heat transfer coefficients under reduced gravity. The current data do approach the Chu and Jones correlation at larger two-phase Reynolds numbers, but the differences are still significant.

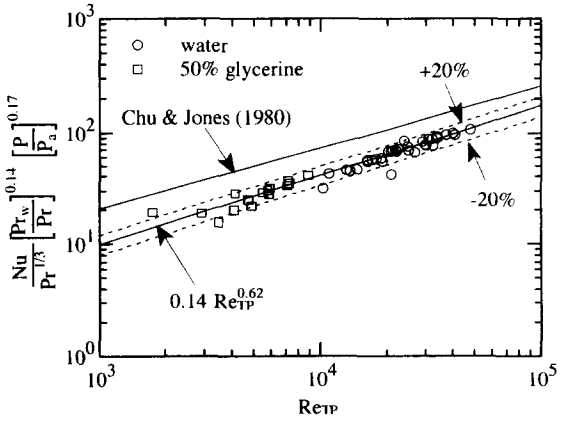

Figure 10. Correlation of heat transfer coefficients with Chu and Jones (1980) formulation.

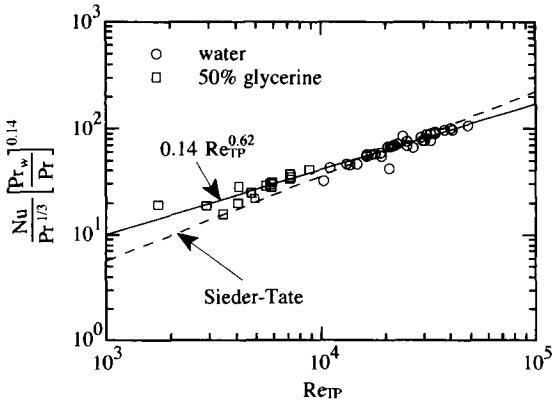

Figure 11. Comparison of Nusselt numbers with Sieder–Tate (1936) correlation based on the two-phase Reynolds number.

While the experimental Nusselt numbers do not agree with the Chu and Jones correlation, they follow a definite relationship with the two-phase Reynolds number. This can be explained by considering the origin of this parameter. Neglecting the exchange of heat between the gas and liquid phases, axial conduction and radial convection, the time-averaged convection–conduction equation for the liquid phase is written as

$$u\frac{\partial T}{\partial x} = \frac{1}{r}\frac{\partial}{\partial r}\left[r\left(\frac{k}{\rho C_p} + \epsilon_h\right)\frac{\partial T}{\partial r}\right], \qquad [10]$$

where u is the local axial liquid velocity, ρ is the liquid density and ϵ_h is the eddy thermal diffusivity. With this simplified model, heat transfer is enhanced by two mechanisms, an increase in the liquid velocity and an increase in the eddy diffusivity. The gas bubbles displace the liquid, leading to increases in u, while the slip between the bubbles and liquid increase turbulence levels, leading to increases in the eddy diffusivity. The natural length scale for this equation is the tube diameter and the natural velocity scale is the mean liquid velocity, which differs from the superficial velocity as

$$U_L = \frac{U_{LS}}{(1-\epsilon)}. \qquad [11]$$

Using these scaling parameters and an arbitrary scale for the temperature, [10] becomes

$$u'\frac{\partial T'}{\partial x'} = \frac{(1-\epsilon)}{Re_L}\frac{1}{r'}\frac{\partial}{\partial r'}\left[r'\left(\frac{1}{Pr} + \frac{\epsilon_h}{\nu}\right)\frac{\partial T'}{\partial r'}\right], \qquad [12]$$

with primes denoting dimensionless quantities. The Reynolds number, Re_L, is the standard based on the wetted perimeter. Equation [12] thus provides an analytical basis for the use of the Chu and Jones two-phase Reynolds number, which is actually a combination of two dimensionless groups from the convection-conduction equation. Using this reasoning, the experimental Nusselt numbers are compared directly to the Sieder–Tate correlation,

$$Nu = 0.023\, Re_{TP}^{0.8}\, Pr^{1/3}\left(\frac{Pr}{Pr_w}\right)^{0.14}, \qquad [13]$$

in figure 11. The present data compare remarkably well with the single-phase turbulent correlation, especially at the higher Reynolds numbers where the Sieder–Tate correlation is usually considered valid. This result suggests that the average eddy diffusivity for these experiments is similar to that for single-phase liquid flow at the two-phase Reynolds number. It also provides an explanation for the difference between reduced- and normal-gravity Nusselt numbers. The local liquid velocity should be similar for reduced- and normal-gravity slug flows at the same void fraction, since it is governed by a mass balance and the radial void distribution. The eddy diffusivity may be

significantly different, however, due to differences in gas–liquid slip. Buoyancy-induced slip increases liquid-phase turbulence and with it, the eddy diffusivity. Buoyancy is diminished at reduced gravity, so it is logical that the eddy diffusivity would also be smaller. Based on this reasoning, the Nusselt numbers measured in this study are smaller than those obtained under normal gravity because the eddy diffusivity is smaller without buoyancy-induced slip.

4. CONCLUSION

New hydrodynamic and heat transfer measurements were made for two-phase slug flows in a reduced gravity environment. The gas-to-mixture velocity ratio approaches the void fraction at low void fractions, representing a nearly homogeneous condition. At higher void fractions, the velocity ratio increases to values consistent with those obtained in ground-based vertical experiments, minus the effect of buoyancy-induced slip. The enhancement of the heat transfer coefficient over single-phase flow increases with increasing void fraction, and is somewhat larger for a 50% glycerine solution as opposed to pure water. The measured heat transfer coefficients are lower at reduced-gravity than predicted by normal-gravity correlations. This difference can be accounted for by the lower turbulence levels that should exist without the effect of buoyancy in reduced gravity.

Acknowledgements—This work was supported by the NASA Lewis Research Center under grant NAG3-510. Special thanks are due to the Lewis team of G. Fedor, S. Fisher, T. Lorik and M. Shoemaker, and to R. Mate at the University of Houston.

REFERENCES

Bousman, W. S. (1994) Studies of two-phase gas–liquid flow in microgravity. Ph.D. dissertation, University of Houston; also: NASA Contractor Report 195434 (1995).

Bousman, W. S. and Dukler, A. E. (1994) Ground based studies of gas–liquid flows in microgravity using lear jet trajectories. Paper AIAA 94-0829, 32nd Aerospace Sciences Meeting and Exhibit, Reno, NV.

Chu, Y.-C. and Jones, B. G. (1980) Convective heat transfer coefficient studies in upward and downward, vertical, two-phase, non-boiling flows. *AIChE Symp. Series* **76,** 79–90.

Dorresteijn, W. R. (1970) Experimental study of heat transfer in upward and downward two-phase flow of air and oil through 70-mm tubes. *Proc. 4th Int. Heat Transfer Conf.*, Vol. 5, B5.9.

Dukler, A. E., Fabre, J. A., McQuillen, J. B. and Vernon, R. (1988) Gas–liquid flow at microgravity conditions: flow patterns and their transitions. *Int. J. Multiphase Flow* **14,** 389–400.

Elamvaluthi, G. and Srinivas, N. S. (1984) Two-phase heat transfer in two component vertical flows. *Int. J. Multiphase Flow* **10,** 237–242.

Fore, L. B. and Witte, L. C. (1995) Roll-wave effects on the heating of viscous liquid films. *Proc. 30th Nat. Heat Transfer Conf.*, HTD-Vol. 314, pp. 23–30.

Fried, L. (1954) Pressure drop and heat transfer for two-phase, two-component flow. *Chem. Eng. Prog. Symp. Series* **50,** 47–51.

Kudirka, A. A., Grosh, R. J. and McFadden, P. W. (1965) Heat transfer in two-phase flow of gas–liquid mixtures. *Ind. Eng. Chem. Fundam.* **4,** 339–344.

Lacy, C. E. and Dukler, A. E. (1994) Flooding in vertical tubes—I. Experimental studies of the entry region. *Int. J. Multiphase Flow* **20,** 219–233.

Moffat, R. J. (1988) Describing the uncertainties in experimental results. *Experimental Thermal and Fluid Science* **1,** 3–17.

Rite, R. W. and Rezkallah, K. S. (1993) An investigation of transient effects on heat transfer measurements in two-phase, gas–liquid flow under microgravity conditions. *Proc. 29th National Heat Transfer Conf.: Heat Transfer in Microgravity Systems*, HTD-Vol. 235, pp. 49–57.

Rite, R. W. and Rezkallah, K. S. (1994) Heat transfer in two-phase flow through a circular tube at reduced gravity. *Journal of Thermophysics and Heat Transfer* **8,** 702–708.

Shah, M. M. (1981) Generalized prediction of heat transfer during two component gas–liquid flow in tubes and other channels. *AIChE Symp. Ser.* **77,** 141–151.

Sieder, E. N. and Tate, G. E. (1936) Heat transfer and pressure drop of liquids in tubes. *Ind. Eng. Chem.* **28,** 1428–1436.

Vijay, M. M., Aggour, M. A. and Sims, G. E. (1982) A correlation of mean heat-transfer coefficients for two-phase two-component flow in a vertical tube. *Proc. 7th Int. Heat Transfer Conf.*, Munich, Vol. 5, pp. 367–372.

Zhao, L. and Rezkallah, K. S. (1993) Gas–liquid flow patterns at microgravity conditions. *Int. J. Multiphase Flow* **19**, 751–763.

Zuber, N. and Findlay, J. A. (1965) Average volumetric concentration in two phase systems. *J. Heat Transfer* **87,** 453–468.